TITLE:

Phase correction method in a wide detector plane for MIEZE spectroscopy with pulsed neutron beams

AUTHOR(S):

Oda, Tatsuro; Endo, Hitoshi; Ohshita, Hidetoshi; Seya, Tomohiro; Yasu, Yoshiji; Nakajima, Taro; Hino, Masahiro; Kawabata, Yuji

Phase correction method in a wide detector plane for MIEZE spectroscopy with pulsed neutron beams

Check for updates

Tatsuro Oda [a,*], Hitoshi Endo [b], Hidetoshi Ohshita [b], Tomohiro Seya [b], Yoshiji Yasu [b], Taro Nakajima [c,d], Masahiro Hino [a], Yuji Kawabata [a]

[a] *Institute for Integrated Radiation and Nuclear Science, Kyoto University, Kumatori, Osaka 590-0494, Japan*
[b] *Institute of Materials Structure Science, High Energy Accelerator Research Organization, Tokai, Ibaraki 319-1195, Japan*
[c] *Institute for Solid State Physics, University of Tokyo, Kashiwa, Chiba 277-8581, Japan*
[d] *RIKEN Center for Emergent Matter Science (CEMS), Wako, Saitama 351-0198, Japan*

ARTICLE INFO

ABSTRACT

In this study, we propose a phase correction method for a type of neutron spin echo spectroscopy, known as modulation of intensity with zero effort using a time-of-flight method (TOF-MIEZE). The phase of the MIEZE signal sensitively varies with the neutron flight path lengths. The geometrical lengths from the sample position to the flat detector plane differ depending on the positions on the detector plane. Integrating the phase-shifted signals may decrease the signal contrast solely through the geometrical path-length deviations. To measure the decrement of contrast accurately, which corresponds to the intermediate scattering function, the position-dependent phase shifts must be corrected. The data correction is performed by shifting the MIEZE signal in time depending on path-length deviations, the MIEZE frequency, and neutron wavelengths. In the calculation of path-length deviations, the sample is assumed to be a point scatterer while a detector inclination is taken into account. We also discuss the relation between the frequency shift of TOF-MIEZE signal and path-length deviation, which is helpful to quantify phase shifts larger than 2π. The presented phase correction method is demonstrated with a 32×32 cm^2 area detector for a 200 kHz TOF-MIEZE signal scattered from an elastic sample.

1. Introduction

In neutron spin echo (NSE) spectroscopy [1,2], the dynamical property of samples is analyzed through the intermediate scattering function $I(Q, \tau)$, which is observed as a decrease in contrast of the spin echo signal. The echo signals result from the interference of superposition states of spin-polarized neutrons. Their oscillating part is generally represented by a sinusoidal function, $f(\phi) = B + A \sin \phi$, the phase ϕ of which is dependent on the neutron wavelength and instrumental setup. A contrast of the signal, also referred to as visibility, is given by the ratio of the amplitude A and the base intensity B: $C = A/B$.

In a type of NSE technique, called modulation of intensity with zero effort (MIEZE) [3,4], time-modulated signals are generated by multiple resonant spin flips. The phase of MIEZE signal is highly dependent on the flight path length of neutrons. Therefore, unless neutron detectors have a perfect spherical surface centered on the sample, the signal phases may vary at different detector pixels. Integrating the phase-shifted signals may degrade the MIEZE signal regardless of the dynamics of the sample.

For the MIEZE implementation using a quasi-monochromatic continuous neutron beam, the position-dependent phase problem and a correction method have been reported [5] from the RESEDA instrument [6,7] at a reactor source of Heinz Maier-Leibnitz Zentrum (MLZ), Germany. Accuracy of detector positioning required to maintain a contrast increases with the frequency of MIEZE signal [8]. With a pulsed neutron beam, the required accuracy is generally relaxed because the wavelength resolution can be higher than that of a continuous beam ($\Delta\lambda/\lambda \sim 10\%$). The MIEZE technique using pulsed neutron beams (TOF-MIEZE) is currently implemented at BL06 VIN ROSE [9] at the Materials and Life Science Experimental Facility (MLF) [10] of the Japan Proton Accelerator Research Complex (J-PARC) and the Larmor instrument [11] at the ISIS Neutron and Muon Source, UK.

Recently, we have started the operation of a neutron detector with a wide effective area of 32×32 cm^2 at BL06 to cover more solid angles and allow efficient use of the polychromatic pulsed beams. In this paper, we report on a phase correction method for the TOF-MIEZE signal required for the MIEZE instrument with the wide area detectors. We derive an analytical expression of the path-length deviation in a
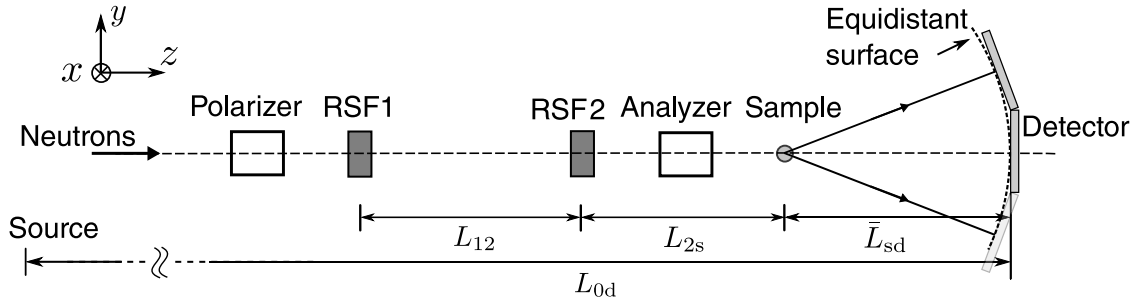
Fig. 1. Schematic of a MIEZE-type NSE instrument.

general configuration of a detector. This is useful for reproducing the phase shifts with a few parameters and embedding the phase correction in the data reduction process. We also discuss the correspondence between the frequency shifts of TOF-MIEZE signal and path-length deviations, which is helpful to determine a detector configuration. With the above findings, we demonstrate the phase correction method for polychromatic pulsed neutrons measured by a wide area detector.

The presented correction scheme is valid for the non-dispersive phase shifts that arise on different detector pixels. We neglect the effect of a finite sample volume and finite beam size and divergence in the scheme. The distribution of neutron path lengths is considered to be a convolution of these effects and scattering directions. Unless there is significant anisotropy, the center of the distribution should be close to that of the case with a point-like sample and infinitely collimated beam. Dispersion of the distribution, for which our correction method is not applicable, can be problematic even when using a high wave-length resolution. The dispersion caused by a sample volume has been studied analytically [12] and by numerical simulations [13,14]. Several systems using focusing optics have been proposed to reduce the path-length dispersion from a beam divergence while maintaining the beam intensity [14–16].

2. Phase correction method for MIEZE spectroscopy

We consider a simple MIEZE setup with two resonance spin flippers (RSFs), RSF1 and RSF2, driven with frequencies of ω_1 and ω_2, respectively. Figure 1 shows a schematic of the setup. The phase of the MIEZE signal can be expressed as the follows [17]:

$$\phi(v, t) = \omega_1 \frac{L_{12}}{v} - \omega_M \frac{L_{2s} + L_{sd}}{v} + \omega_M t + \chi, \qquad (1)$$

where v denotes the neutron velocity, L_{12} is the distance between RSF1 and RSF2, L_{2s} is the distance between RSF2 and the sample, L_{sd} is the distance between the sample and the detector, $\omega_M = \omega_2 - \omega_1$ and χ is a constant affected by the phases of radiofrequency (RF) currents of RSFs. We assume the MIEZE condition is satisfied with a certain $L_{sd} = \bar{L}_{sd}$,

$$\omega_1 L_{12} = \omega_M (L_{2s} + \bar{L}_{sd}). \qquad (2)$$

In this condition, the phase of the MIEZE signal is independent of the neutron velocity (wavelength), and the signal can be expressed as

$$I(t_d) \propto \frac{1}{2} \left[1 + \cos(\omega_M t_d + \chi) \right]. \qquad (3)$$

Before taking the sample measurements, the apparatus is tuned to the MIEZE condition with the incident neutron beam. However, the path lengths L_{sd} of scattered neutrons may differ from point to point unless the detector plane is a perfect sphere centered on the sample. With a path-length deviation, $L_{sd} = \bar{L}_{sd} + \Delta L_{sd}$, the phase shift is given by

$$\Delta\phi = \omega_M \frac{\Delta L_{sd}}{v} = \omega_M \Delta t, \quad \Delta t = \frac{\Delta L_{sd}}{v}. \qquad (4)$$

Once the path-length deviations ΔL_{sd} are known, one can perform phase correction according to Eq. (4). Specifically, to compensate for the phase shifts, the recorded detection time t_d should be shifted to $t_d - \Delta t$ before drawing the time histogram (see Fig. 2(c)).
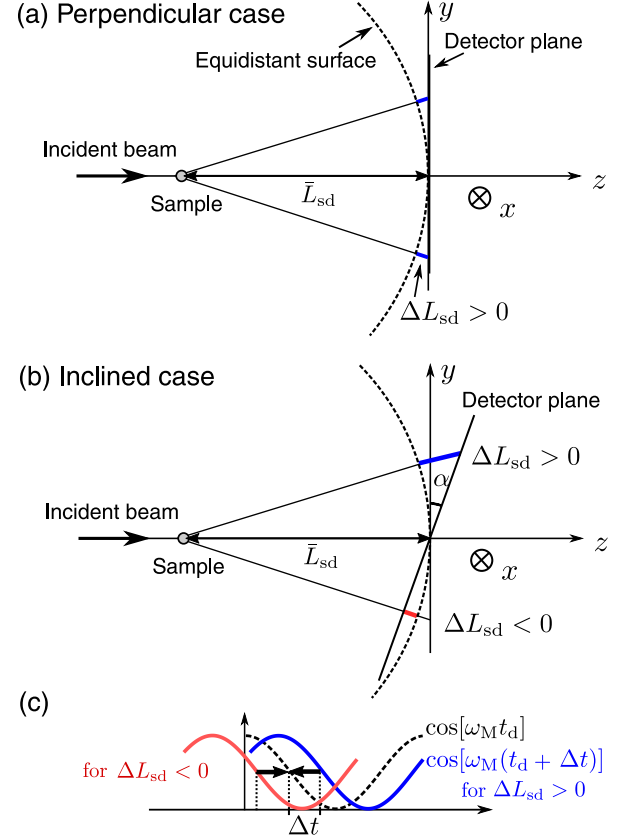

Fig. 2. Path-length deviations in (a) perpendicular and (b) inclined configurations. (c) MIEZE signals with phase shifts.

2.1. Path-length deviations

Here we derive the position dependence of the path-length deviations in a flat detector plane. We first consider the case in which the detector plane is perpendicular to the beam direction as shown in Fig. 2(a). We assume that the MIEZE condition is satisfied at the center of the detector $(x', y') = (0, 0)$ with a distance $L_{sd} = \bar{L}_{sd}$. The path-length deviation at (x', y') on the detector plane is given by

$$\Delta L_{sd} = \sqrt{\bar{L}_{sd}^2 + x'^2 + y'^2} - \bar{L}_{sd} \simeq \frac{x'^2 + y'^2}{2\bar{L}_{sd}}. \qquad (5)$$

In the perpendicular case, $\Delta L_{sd} \geq 0$ for any (x', y').

Second, we consider a more general configuration of the detector: the detector plane has inclinations α and β around the x- and y-axis, respectively ($|\alpha|, |\beta| \ll 1$). For high MIEZE frequencies, non-negligible path-length deviations can be caused by inclinations of the order of $0.1°$, which are inherent in practical experimental alignment.
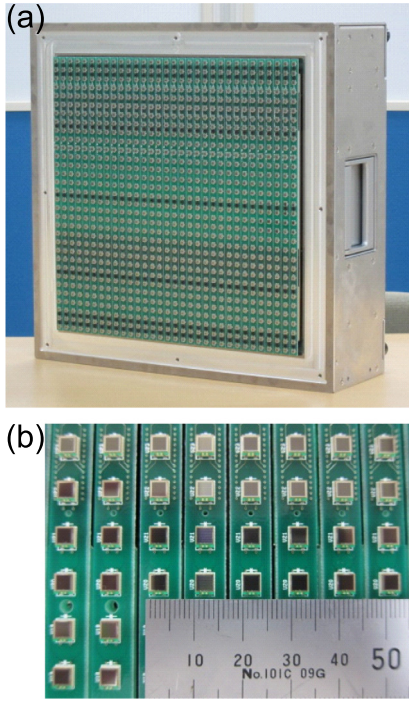
Fig. 3. (a) Photograph of a Mpix detector with an effective area of 32×32 cm^2 (a scintillator plate and aluminum cover are removed). (b) Multi-pixel photon counters are arranged regularly in an interval of 1 cm.

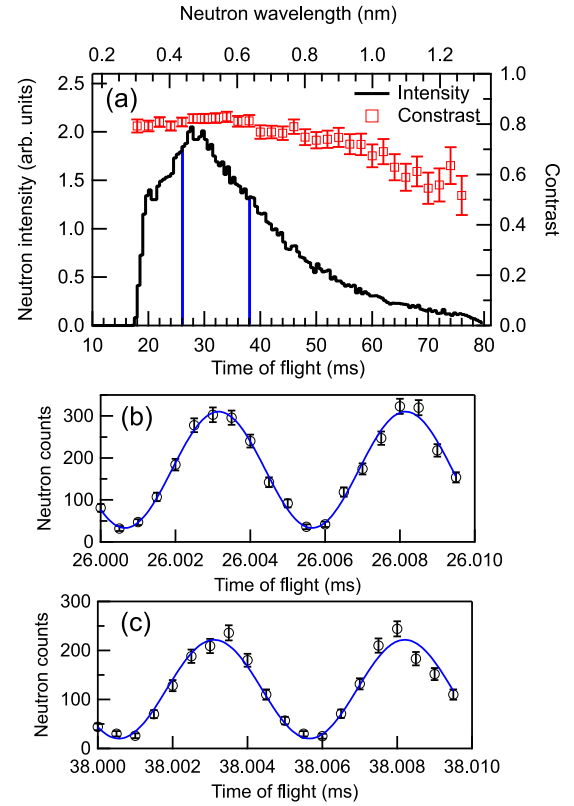**Fig. 4.** (a) TOF spectrum of the incident beam and the contrast of the 200 kHz MIEZE signal. The bin width of TOF spectrum is 500 μs (b) Examples of individual MIEZE oscillations at TOF ranges of (b) 26.00–26.01 ms and (c) 38.00–38.01 ms. The time bin width is 0.5 μs.

We denote the position in the laboratory coordinate system by $\boldsymbol{r} = x\boldsymbol{e}_x + y\boldsymbol{e}_y + z\boldsymbol{e}_z$, and the local coordinate on the detector plane by $\boldsymbol{r} = x'\boldsymbol{e}'_x + y'\boldsymbol{e}'_y$. Here $\boldsymbol{e}_j$ and $\boldsymbol{e}'_j$ denote orthonormal basis vectors in each coordinate system. In the measurement data, (x', y') is recorded. In the following analysis, subscripts $\{1, 2, 3\}$ are read as $\{x, y, z\}$. In general, $\boldsymbol{e}'_j$ $(j = 1, 2, 3)$ can be expressed as a linear combination of $\{\boldsymbol{e}_1, \boldsymbol{e}_2, \boldsymbol{e}_3\}$. The coefficients are given by the elements of the following rotation matrix:

$$R^{-1} = R_x^{-1}(\alpha) R_y^{-1}(\beta) = \begin{pmatrix} \cos\beta & 0 & -\sin\beta \\ \sin\alpha\sin\beta & \cos\alpha & \sin\alpha\cos\beta \\ \cos\alpha\sin\beta & -\sin\alpha & \cos\alpha\cos\beta \end{pmatrix}, \quad (6)$$

where R_x and R_y are the rotation matrices around x- and y-axis, respectively:

$$R_x(\alpha) = \begin{pmatrix} 1 & 0 & 0 \\ 0 & \cos\alpha & -\sin\alpha \\ 0 & \sin\alpha & \cos\alpha \end{pmatrix}, \quad R_y(\beta) = \begin{pmatrix} \cos\beta & 0 & \sin\beta \\ 0 & 1 & 0 \\ -\sin\beta & 0 & \cos\beta \end{pmatrix}. \quad (7)$$

Thus, $\boldsymbol{r}$ can be written in the laboratory coordinate system as follows:

$$\boldsymbol{r} = x'\boldsymbol{e}'_1 + y'\boldsymbol{e}'_2 = x' \sum_j^3 R_{1j}^{-1}\boldsymbol{e}_j + y' \sum_j^3 R_{2j}^{-1}\boldsymbol{e}_j$$

$$= \begin{pmatrix} x'\cos\beta + y'\sin\alpha\sin\beta \\ y'\cos\alpha \\ -x'\sin\beta + y'\sin\alpha\cos\beta \end{pmatrix}. \quad (8)$$

The path-length deviation $\Delta L_{\mathrm{sd}}(x', y')$ is calculated as

$$\Delta L_{\mathrm{sd}} = |\boldsymbol{r} - (-\bar{L}_{\mathrm{sd}}\boldsymbol{e}_z)| - \bar{L}_{\mathrm{sd}}$$
$$= \big[(x'\cos\beta + y'\sin\alpha\sin\beta)^2 + (y'\cos\alpha)^2$$
$$+ (\bar{L}_{\mathrm{sd}} - x'\sin\beta + y'\sin\alpha\cos\beta)^2 \big]^{1/2} - \bar{L}_{\mathrm{sd}}$$
$$= \big[(x' - \bar{L}_{\mathrm{sd}}\sin\beta)^2 + (y' + \bar{L}_{\mathrm{sd}}\sin\alpha\cos\beta)^2$$
$$+ \bar{L}_{\mathrm{sd}}^2 \cos^2\alpha \cos^2\beta \big]^{1/2} - \bar{L}_{\mathrm{sd}}. \quad (9)$$

One can see that ΔL_{sd} takes its minimum value, $-\bar{L}_{\mathrm{sd}}(1 - \cos\alpha\cos\beta)$ at $(x', y') = (\bar{L}_{\mathrm{sd}}\sin\beta, -\bar{L}_{\mathrm{sd}}\sin\alpha\cos\beta)$. To compensate for a small

misalignment from the MIEZE condition, we add a length offset ℓ to the fitting model, that is,

$$\Delta L_{\mathrm{sd}}(x', y'; \alpha, \beta, \ell) = \big[(x' - \bar{L}_{\mathrm{sd}}\sin\beta)^2 + (y' + \bar{L}_{\mathrm{sd}}\sin\alpha\cos\beta)^2$$
$$+ \bar{L}_{\mathrm{sd}}^2 \cos^2\alpha \cos^2\beta \big]^{1/2} - (\bar{L}_{\mathrm{sd}} + \ell). \quad (10)$$

A reliable method to determine the configuration parameters α, β, and ℓ is to measure the MIEZE signal from an elastic scattering sample in the actual setup. Once this calibration measurement is performed, we can reproduce ΔL_{sd} and, consequently, Δt in a general configuration using the analytical model.

2.2. Relation between path-length deviations and frequency shifts of TOF-MIEZE signals

A standard approach to measure the path-length deviations is to use the phase shift Eq. (4) with a monochromatic wavelength range. In this measurement the neutron wavelength and MIEZE frequency should be chosen so that the maximum phase shift in a detector area does not exceed 2π [5]. Here, we describe how the frequency shifts of TOF-MIEZE signals can be an alternative approach that is available for phase shifts over 2π.

Including the cases deviating from the MIEZE condition, the TOF-MIEZE signal can be expressed by [17]

$$\frac{1}{2}\left\{ 1 + \cos[(\omega_{\mathrm{M}} - \Omega)t_{\mathrm{d}} + \chi] \right\}, \quad (11)$$

where the frequency shift Ω is defined as [18]

$$\Omega = \frac{-\omega_1 L_{12} + \omega_{\mathrm{M}}(L_{2\mathrm{s}} + L_{\mathrm{sd}})}{L_{0\mathrm{d}}}. \quad (12)$$
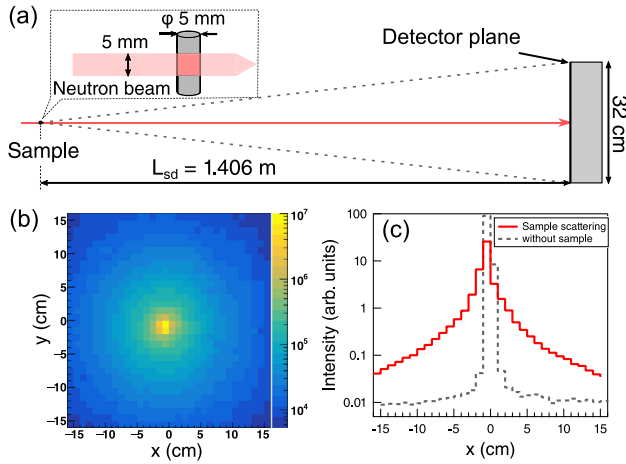
Fig. 5. (a) Setup of the calibration measurement with a diamond powder sample. The inset shows dimensions of the sample and the incident neutron beam. (b) Two-dimensional intensity distribution of scattered and transmitted neutrons. (c) Horizontal projections of intensity with the sample (solid line) and without sample (dashed line).
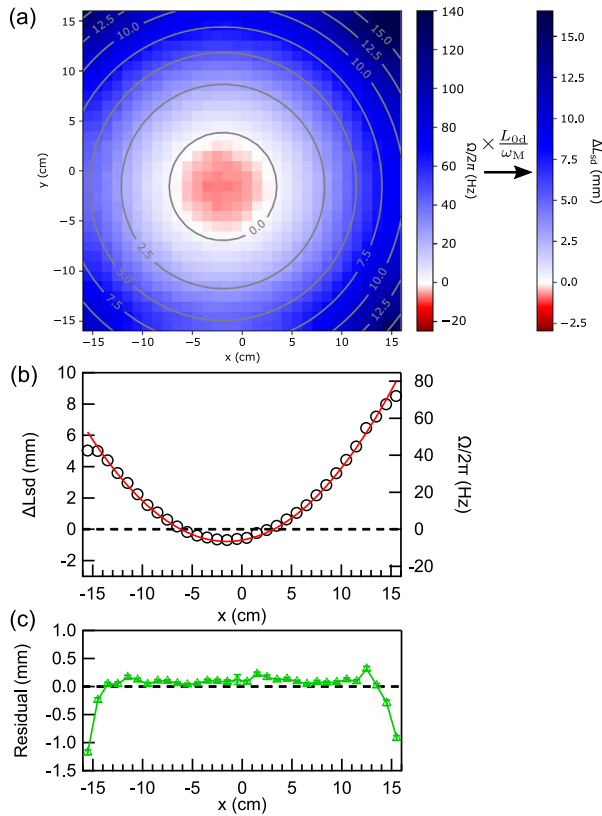

Fig. 6. (a) Observed position dependence of the frequency shift Ω and corresponding path-length deviation $\Delta L_{sd} = (\Omega/\omega_M)L_{0d}$. The contour lines show the two-dimensional fitting result by Eq. (10). (b) The x-position dependence of Ω and ΔL_{sd} on the line $y = 0$. The black circles show the measurement data, and the red solid line is the best-fit curve. (c) The difference between the measurement data and best-fit curve.

In the MIEZE condition Eq. (2), where $L_{sd} = \bar{L}_{sd}$, we have $\Omega = 0$. With a path-length deviation, $L_{sd} \rightarrow \bar{L}_{sd} + \Delta L_{sd}$, we have non-zero Ω, and ΔL_{sd} is given by

$$\Delta L_{sd} = \frac{\frac{\Omega}{\omega_M}\bar{L}_{0d}}{1 - \frac{\Omega}{\omega_M}} \simeq \frac{\Omega}{\omega_M}\bar{L}_{0d}. \tag{13}$$

The approximation follows by $\Omega/\omega_M \ll 1$. Here $\bar{L}_{0d}$ denotes the total flight path length for the case of $L_{sd} = \bar{L}_{sd}$. From this relation, path-length deviation ΔL_{sd} can be calculated by measuring Ω instead of signal phases. This is because, in the TOF-MIEZE method, the information regarding phase shifts for all available wavelengths is incorporated into Ω. More importantly, the frequency shift can quantify large path-length deviations, overcoming the 2π periodicity in phase shifts. This feature comes from the width of the wavelength band used in the TOF-MIEZE method. By mapping the frequency shifts on the detector plane, we can easily measure the path-length deviations required for the phase correction. Following the approach based on frequency shifts, the phase correction procedure is as follows.

1. (Calibration measurement) Record the TOF-MIEZE signal on the whole detector plane with an elastic scattering sample.
2. Evaluate the frequency shifts Ω of the TOF-MIEZE signal in each spatial bin and convert Ω into ΔL_{sd} by multiplying by a factor L_{0d}/ω_M (Eq. (13)).
3. Fit the two-dimensional ΔL_{sd} map and determine the parameters α, β, and ℓ of Eq. (10).
4. Calculate ΔL_{sd} and Δt for each neutron detection event and draw a time histogram with shifted time $t_d - \Delta t$.

The resulting time histogram represents a MIEZE signal without the dephasing effect of path-length deviations on the detector plane.

3. Experimental demonstration

To demonstrate the presented phase correction method, we performed an experiment using the MIEZE-type NSE instrument at BL06 at MLF J-PARC. We used a position- and time-sensitive neutron detector, named Mpix, developed at the Institute of Materials Structure Science (IMSS), High Energy Accelerator Research Organization (KEK). The detector is composed of a 32×32 array of silicon photomultipliers (multi-pixel photon counters; MPPC, Hamamatsu Photonics K.K) and a ^{6}LiF/ZnS(Ag) scintillator plate. We used ZnS scintillator for the availability of products with large areas. The photomultiplier pixels are arranged at an interval of 1 cm to cover an effective area of 32×32 cm^2 as shown in Fig. 3. For the current implementation of the Mpix detector, the spatial resolution (1×1 cm^2) is determined by the pixel interval. It can be improved by the weighted center calculation with additional analog-to-digital (A/D) converters. Event-based data acquisition was performed by the NeuNET module [19]. In the event-data format, measured values of position, time-of-flight (TOF), time stamp, and other parameters are recorded for each neutron detection event. The data process of phase correction was applied to the individual event before drawing a time histogram of the MIEZE signal. Therefore, the resolution of time-shifting for correction and the time bin width for drawing the MIEZE signal are decoupled.

The MIEZE setup consisted of two resonant spin flippers driven by the RFs $\omega_1/2\pi = 200$ kHz and $\omega_2/2\pi = 400$ kHz. The resulting MIEZE frequency was $\omega_M/2\pi = (\omega_2 - \omega_1)/2\pi = 200$ kHz. The alignments of the setup were $L_{0d} = 23.64$ m, $L_{12} = 2.880$ m, $L_{2s} = 0.970$ m, $\bar{L}_{sd} = 1.406$ m. The length of $\bar{L}_{sd}$ from the sample to the detector center was measured by a laser distance meter after an alignment for the MIEZE condition referencing the frequency shifts. Figure 4 shows a typical 200 kHz TOF-MIEZE signal of the incident beam in the setup. Panel (a) shows the TOF spectrum and the contrast of the MIEZE signal in a time frame of 80 ms, whereas panels (b) and (c) show examples of sinusoidal oscillations in two MIEZE periods (10 μs) for neutron wavelengths $\lambda = 0.45$ and 0.65 nm, respectively. The fitting curve and the signal contrast shown in Fig. 4 are

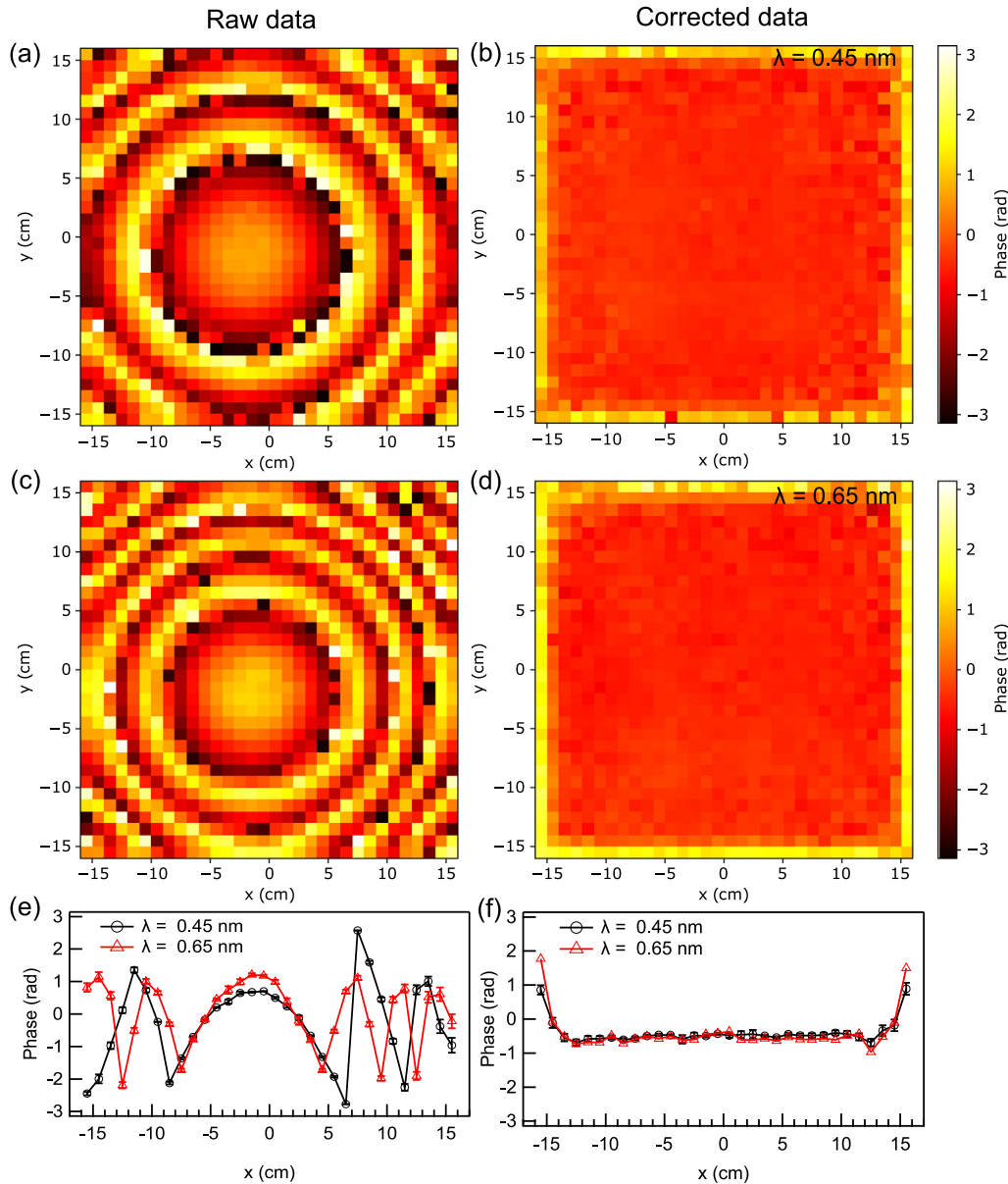$$f(t) = B + A\cos(\omega_M t + \chi), \tag{14a}$$

$$C = \frac{A}{B}. \tag{14b}$$

Fig. 7. The left (a,c,e) and right (b,d,f) column show the raw data and phase corrected data, respectively. Raw phase maps of the $200\,\text{kHz}$ MIEZE signal for the neutron wavelength (a) $\lambda = 0.45$ nm and (c) $\lambda = 0.65$ nm. Phase maps after correction for (b) $\lambda = 0.45$ nm and (d) $\lambda = 0.65$ nm. Typical x-position dependence of the signal phase at $y = 0$ (e) without and (f) with the phase correction. The phase values are wrapped into $[-\pi, \pi]$.

The calibration measurement to determine the detector configuration parameters (α, β, and ℓ) was performed with a polycrystalline diamond powder (Microdiamant AG). The measurement setup is sketched in Fig. 5(a). The powder sample was filled in a cylindrical cell with an inner diameter of $5\,\text{mm}$ and height of $20\,\text{mm}$. The beam size at the sample was approximately $5 \times 5\,\text{mm}^2$. Figure 5(b, c) shows the intensity distribution of scattered neutrons. Because of its wide specific interfacial area of powder form, the sample showed reasonably strong scattering signals to illuminate the full area of the detector plane for phase mapping.

The frequencies of TOF-MIEZE signal in each spatial bin were determined by the peak position of the power spectral obtained by the Fourier transform. Figure 6(a) shows the map of observed frequency shifts and path-length deviations converted by Eq. (13).

The contour lines show the two-dimensional fitting result by Eq. (10). The fitting parameters were determined as $\alpha = 0.76(1)°$, $\beta = -0.60(1)°$, and $\ell = 0.64(1)$ mm. The non-zero value of ΔL_{sd} at the center

$(x, y) = (0,0)$ means that the first alignment for the MIEZE condition by the incident beam was imperfect. The offset ℓ accounts for this misalignment. Because we found a clear discrepancy between the fitting model and experimental data on the edge of the detector, we excluded the two edge bins from the fitting. As an example, a data slice at the $y = 0$ line is shown in Fig. 6(b). The observed ΔL_{sd} and best fit curve show a good agreement except for two points on the edge. Figure 6(c) shows the residual between the fitting model and experimental data.

Figure 7 shows the phase maps of the MIEZE signal without (panels (a,c,e)) and with the phase correction (panels (b,d,f)). To illustrate the wavelength-dependence of the phase variation, we show data for two different wavelengths ($\lambda = 0.45$ and 0.65 nm) that have sufficient scattered signal statistics. Without phase correction, the phase of the MIEZE signal changes drastically in the position and phase shifts over 2π were observed out of the central part ($|x| > 5\,\text{cm}$). With phase correction, the phase becomes constant for wavelengths and positions except in the edge pixels of the detector.

4. Conclusion

A phase correction method for TOF-MIEZE spin echo signals in a flat detector plane was presented. The path-length deviations in a general configuration of the detector were derived. The frequency shift of the TOF-MIEZE signal is a good indicator for the path-length deviations, whereas the phase shift has indefiniteness by 2π periodicity for large deviations. The presented phase correction method was demonstrated with measurement data from an elastic scatter with a 32×32 cm^2 detector. The phase correction was performed by shifting the detection time of each event. The corrected data showed good phase uniformity over most of the detection area. The wide solid angles ensured by the phase correction are important for the efficient use of broadband pulsed neutron beams in TOF-MIEZE spectroscopy.

CRediT authorship contribution statement

Tatsuro Oda: Conceptualization, Methodology, Software, Investigation, Writing - original draft. **Hitoshi Endo:** Conceptualization, Investigation. **Hidetoshi Ohshita:** Resources, Investigation. **Tomohiro Seya:** Resources, Data curation. **Yoshiji Yasu:** Resources, Data curation. **Taro Nakajima:** Conceptualization, Methodology. **Masahiro Hino:** Conceptualization, Supervision. **Yuji Kawabata:** Supervision.

Declaration of competing interest

The authors declare that they have no known competing financial interests or personal relationships that could have appeared to influence the work reported in this paper.

Acknowledgments

References

[1] F. Mezei, Neutron spin echo: A new concept in polarized thermal neutron techniques, Z. Phys. 255 (1972) 146.

[2] F. Mezei (Ed.), Neutron spin echo, Lecture Notes in Physics, vol. 128, Springer-Verlag, Heidelberg, 1980.

[3] R. Gähler, R. Golub, T. Keller, Neutron resonance spin-echo – A new tool for high-resolution spectroscopy, Phys. B 180 (1992) 899–902.

[4] R. Golub, R. Gähler, T. Keller, A plane-wave approach to particle-beam magnetic-resonance, Amer. J. Phys. 62 (9) (1994) 779–788.

[5] A. Schober, A. Wendl, F.X. Haslbeck, J.K. Jochum, L. Spitz, C. Franz, The software package MIEZEPY for the reduction of MIEZE data, J. Phys. Commun. 3 (10) (2019) 103001.

[6] C. Franz, S. Säubert, A. Wendl, F.X. Haslbeck, O. Soltwedel, J.K. Jochum, L. Spitz, J. Kindervater, A. Bauer, P. Böni, C. Pfleiderer, MIEZE neutron spin-echo spectroscopy of strongly correlated electron systems, J. Phys. Soc. Japan 88 (8) (2019) 081002.

[7] C. Franz, O. Soltwedel, C. Fuchs, S. Säubert, F. Haslbeck, A. Wendl, J.K. Jochum, P. Böni, C. Pfleiderer, The longitudinal neutron resonant spin echo spectrometer RESEDA, Nucl. Instrum. Methods A 939 (2019) 22–29.

[8] J.K. Jochum, A. Wendl, T. Keller, C. Franz, Neutron MIEZE spectroscopy with focal length tuning, Meas. Sci. Technol. 31 (3) (2019) 035902.

[9] M. Hino, T. Oda, N.L. Yamada, H. Endo, H. Seto, M. Kitaguchi, M. Harada, Y. Kawabata, Supermirror neutron guide system for neutron resonance spin echo spectrometers at a pulsed neutron source, J. Nucl. Sci. Technol. 54 (11) (2017) 1223–1232.

[10] K. Nakajima, Y. Kawakita, S. Itoh, J. Abe, K. Aizawa, H. Aoki, H. Endo, M. Fujita, K. Funakoshi, W. Gong, M. Harada, S. Harjo, T. Hattori, M. Hino, T. Honda, A. Hoshikawa, K. Ikeda, T. Ino, T. Ishigaki, Y. Ishikawa, H. Iwase, T. Kai, R. Kajimoto, T. Kamiyama, N. Kaneko, D. Kawana, S. Ohira-Kawamura, T. Kawasaki, A. Kimura, R. Kiyanagi, K. Kojima, K. Kusaka, S. Lee, S. Machida, T. Masuda, K. Mishima, K. Mitamura, M. Nakamura, S. Nakamura, A. Nakao, T. Oda, T. Ohhara, K. Ohishi, H. Ohshita, K. Oikawa, T. Otomo, A. Sano-Furukawa, K. Shibata, T. Shinohara, K. Soyama, J.-I. Suzuki, K. Suzuya, A. Takahara, S.-I. Takata, M. Takeda, Y. Toh, S. Torii, N. Torikai, N. Yamada, T. Yamada, D. Yamazaki, T. Yokoo, M. Yonemura, H. Yoshizawa, Materials and life science experimental facility (MLF) at the Japan proton accelerator research complex II: Neutron scattering instruments, Quantum Beam Sci. 1 (3) (2017).

[11] N. Geerits, S.R. Parnell, M.A. Thijs, A.A. van Well, C. Franz, A.L. Washington, D. Raspino, R.M. Dalgliesh, J. Plomp, Time of flight modulation of intensity by zero effort on Larmor, Rev. Sci. Instrum. 90 (12) (2019) 125101.

[12] G. Brandl, R. Georgii, W. Häußler, S. Mühlbauer, P. Böni, Large scales-long times: Adding high energy resolution to SANS, Nucl. Instrum. Methods A 654 (1) (2011) 394–398.

[13] H. Hayashida, M. Hino, M. Kitaguchi, Y. Kawabata, N. Achiwa, A study of resolution function on a MIEZE spectrometer, Meas. Sci. Technol. 19 (3) (2008).

[14] T. Weber, G. Brandl, R. Georgii, W. Häußler, S. Weichselbaumer, P. Böni, Monte-Carlo simulations for the optimisation of a TOF-MIEZE instrument, Nucl. Instrum. Methods A 713 (2013) 71–75.

[15] M. Bleuel, F. Demmel, R. Gähler, R. Golub, K. Habicht, T. Keller, S. Klimko, I. Köper, S. Longeville, S. Prokudaylo, Future developments in resonance spin echo, in: F. Mezei, C. Pappas, T. Gutberlet (Eds.), Neutron Spin Echo Spectroscopy, in: Lecture Notes in Physics, vol. 601, Springer, Berlin, Heidelberg, 2002, pp. 176–200.

[16] F. Funama, S. Tasaki, M. Hino, T. Oda, H. Endo, Double-focusing geometry for phase correction in neutron resonance spin-echo spectroscopy, Nucl. Instrum. Methods A 1010 (2021) 165480.

[17] T. Oda, M. Hino, M. Kitaguchi, P. Geltenbort, Y. Kawabata, Pulsed neutron time-dependent intensity modulation for quasi-elastic neutron scattering spectroscopy, Rev. Sci. Instrum. 87 (10) (2016) 105124.

[18] T. Oda, M. Hino, H. Endo, H. Seto, Y. Kawabata, Tuning neutron resonance spin-echo spectrometers with pulsed beams, Phys. Rev. Applied 14 (5) (2020) 054032.

[19] S. Satoh, S. Muto, N. Kaneko, T. Uchida, M. Tanaka, Y. Yasu, K. Nakayoshi, E. Inoue, H. Sendai, T. Nakatani, T. Otomo, Development of a readout system employing high-speed network for J-PARC, Nucl. Instrum. Methods A 600 (1) (2009) 103–106.